

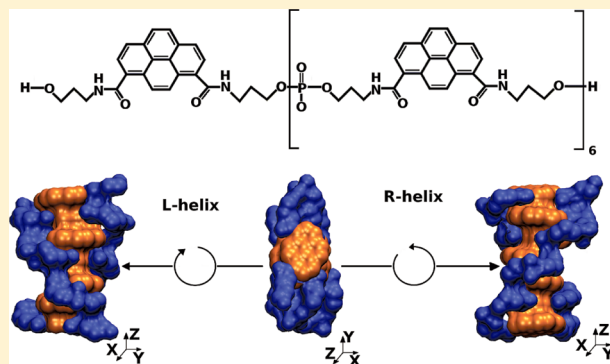
Supramolecular Organization of Heptapyrenotide Oligomers—An in Depth Investigation by Molecular Dynamics Simulations

Fabio Simona, Alina L. Nussbaumer, Robert Häner, and Michele Cascella*

Department of Chemistry and Biochemistry, University of Bern, Freiestrasse 3, 3012 Bern, Switzerland

S Supporting Information

ABSTRACT: We present a molecular modeling study based on ab initio and classical molecular dynamics calculations, for the investigation of the tridimensional structure and supramolecular assembly formation of heptapyrenotide oligomers in water solution. Our calculations show that free oligomers self-assemble in helical structures characterized by an inner core formed by π -stacked pyrene units, and external grooves formed by the linker moieties. The coiling of the linkers has high ordering, dominated by hydrogen-bond interactions among the phosphate and amide groups. Our models support a mechanism of longitudinal supramolecular oligomerization based on interstrand pyrene intercalation. Only a minimal number of pyrene units intercalate at one end, favoring formation of very extended longitudinal chains, as also detected by AFM experiment. Our results provide a structural explanation of the mechanism of chirality amplification in 1:1 mixtures of standard heptapyrenotides and modified oligomers with covalently linked deoxycytidine, based on selective molecular recognition and binding of the nucleotide to the groove of the left-wound helix.



INTRODUCTION

Supramolecular polymers are macromolecules obtained by the self-assembly and self-organization of repeating, non-covalently linked units. Their structural and functional characteristics reside not only in the covalent structure of each monomer, but they are also determined by the nature and directionality of reversible non-covalent interactions among the various components.^{1–3} Development of supramolecular polymers, originally a branch of materials sciences, has recently emerged and grown as a separate field of research.^{4–6}

One of the most important and prominent examples of supramolecular macromolecules in nature are nucleic acids, DNA and RNA, in which the stability of the double helix is attributed to hydrogen bonding between complementary nucleotides and, secondarily, to aromatic π – π stacking of the nucleobases.^{7–9} Many examples of modification and simplification of the nucleic acid structure are present in the literature^{10–14} which are of help to obtain an in depth understanding of the physicochemical properties of nucleic acids, as well as lead to the discovery of new macromolecules, with possible applications in different fields, from materials to medical sciences.^{14–19}

In the past, assembly of polymers driven mainly by hydrogen bond interactions has been extensively explored.^{20–24} On the contrary, the design of polymers whose assembly is governed by aromatic stacking has been investigated to a lesser extent.^{4,6,25} Within this framework, two authors of this work have recently synthesized and experimentally characterized oligomers denoted *heptapyrenotides* (Py₇),²⁶ containing seven

pyrene units^{27,28} (Figure 1A), linked *via* a flexible phosphodiester backbone, and their chemical modifications obtained by adding a terminal 2'-deoxycytidine (called C hereafter) nucleotide (Py₇-C).

Composed of alternating phosphates and poly-aromatic building blocks, these oligopyrenotides represent a kind of simple analogue of oligonucleotides. Like nucleic acids, these water-soluble oligomers fold into organized, probably helical, structures, they are responsive to the ionic strength of the medium, and they can assemble into multistranded aggregates.²⁶

In precedent works,^{27–29} different properties of heptapyrenotides were experimentally characterized. In particular, UV/vis and fluorescence spectroscopy data obtained in an aqueous solution with high ionic strength (i.e., 1 M NaCl) indicated that polymers increase the amount of stacked pyrenes, suggesting salt-induced aggregation of the pyrene units. Moreover, CD spectroscopy for the Py₇ or Py₇-C single polymers did not reveal any distinct signals indicating the presence of a specific chirality, as well as for assembly of Py₇ polymers, while, in a mixture obtained by the addition of small amounts of Py₇-C oligomers to an aqueous solution of Py₇, amplification of chirality was observed. Finally, the additional terminally linked nucleotide can switch the self-assembly of the heptapyrenotides from a cooperative to a noncooperative mechanism.^{27,30–34}

Received: October 18, 2012

Revised: February 1, 2013

Published: February 1, 2013



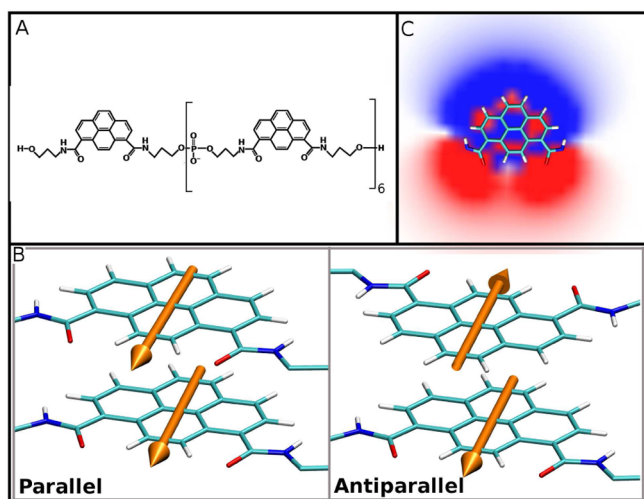


Figure 1. (A) Chemical formula of the heptapyrenotide oligomer. (B) Schematic representation of the two possible relative orientations for consecutive stacking pyrenes. Pyrenes and linked amide units are represented in licorice. The orange arrows represent the molecular electrostatic dipoles associated with the pyrene moieties. (C) 2D map of the molecular electrostatic potential associated with a pyrene base. The profile is produced by the strong dipoles at the amide groups and the induced polarization of the pyrene. The potential was calculated using the same RESP point charges as used in the MD calculations. The blue color represents regions of high positive value of the potential, and the red color represents regions of high negative potential. For the sake of clarity, only atoms belonging to the pyrene and bound amide groups are shown.

Assuming that polymerization occurs by pyrene intercalation, as also confirmed by recent AFM data,³⁵ the structure of a self-assembled fibril can be divided into different domains: (i) regions of the fibril where pyrenes, belonging to distinct heptapyrenotides, are involved in inter-oligomer stacking interactions (*intercalation domains*); (ii) regions where the pyrenes belonging to the same single heptapyrenotide strands assemble independently, therefore resembling single Py₇ (*single oligomer domains*) (Figure 2). Anyway, at present, attempts to obtain high resolution structural information by X-ray and NMR methods failed thus far, and a detailed molecular picture of the structure of Py₇, Py₇-C monomeric units and of their aggregates is still missing.

Knowledge of the structure of these compounds, both as a single oligomer and a supramolecular assembly, would constitute a fundamental step not only to correctly interpret the data available and to provide a rationale for the intriguing properties shown by these compounds, but it may also provide a rational basis for the design of other types of building blocks and oligomers with special structural, optical, and electronic properties.

Here, we present a series of computational studies aimed at addressing the structure of the heptapyrenotides. In particular, we use both quantum and classical molecular dynamics (QM and MD), performed on *in silico* designed structures of the heptapyrenotides, where the only experimental information of stacking of the aromatic rings was used for the preparation of the models. Our results strongly indicate that these compounds assemble in helical structures, as originally postulated.²⁷ The turn of the helices is determined by the folding of the phosphate-dipyrenotide moieties linking two consecutive stacked pyrenes. The corrugation created by these linkers is

also responsible for the formation of two grooves in the folded structure. Given the achirality of the polymer, the two right- and left-wound helices are isoenergetic, and therefore, a 50%–50% racemic mixture is expected to form. Our models of the asymmetric Py₇-C/Py₇ aggregates provide an explanation for the enhancement of the chirality signal detected in the experiment. In particular, interaction between the chiral C nucleotide and the helical groove is key to determining the break of the symmetry of the racemic Py₇ mixture and favors the presence of one specific arrangement over the other.

COMPUTATIONAL METHODS

QM Calculation of Pyrene Stacking. The relative orientation of two consecutive pyrene units was first investigated at the quantum-mechanical level by a minimal model, made by two pyrene rings, joined by a single phosphodiester linker *in vacuo*. Terminal amides at the other ends of the pyrene units were also included in the calculations, and capped with methyl groups. The initial guess geometry was built arranging the pyrenes in a π - π stacked conformation at an interplane distance of 3.5 Å.³⁶

The presence of the linker breaks the symmetry of the electronic structure of the pyrene molecule, and induces an electrostatic dipole in the aromatic moiety (Figure 1C). Therefore, two possible stacking orientations of the pyrenes were considered and tested in our calculations, one in which the dipoles are oriented in parallel and another in antiparallel direction (Figure 1B). The quantum problem was solved at the density-functional-theory level of theory calculations. The generalized gradient approximation was used for the exchange-correlation function, using Becke and Lee–Yang–Parr functionals.^{37–39} Core electrons were replaced by GTH pseudopotentials and the valence ones described using a split-valence augmented double- ζ basis set.^{40–42} Dispersion-corrected atomic centered potentials (DCACP) were used to account for dispersion interactions.^{43–45} The system was placed in a $20 \times 20 \times 20$ Å³ periodic box, and long-range interactions treated according to ref 46. Several cycles of Born–Oppenheimer molecular dynamics (time step $\Delta t = 0.5$ fs) with simulated annealing were repeated. A rescaling thermostat⁴⁷ with 0.999 for cooling the system, and 1.001 for heating it, was used for the annealing, in order to determine minimal energy structures for the dimer. Calculations were run using the CP2K package.⁴⁸

MD Calculations. Classical MD calculations were performed on different models, namely, (i) the single Py₇ and (ii) the single Py₇-C filaments and (iii) the Py₇/Py₇ and (iv) the Py₇-C/Py₇ complexes. The starting models of the single Py₇ oligomers were built following this scheme: First, seven pyrenes were displaced in a stacked conformation at an interplane distance of 3.5 Å, with their longitudinal axes aligned to optimize dispersion interactions. Two extreme situations were considered here: one in which the dipole moments of consecutive pyrenes were organized in an antiparallel pattern and another with all the dipole moments oriented in parallel. Then, the linker groups connecting the pyrene moiety were modeled to complete the structure of the full oligomer. The models for the Py₇-C oligomers were prepared starting from the final relaxed structure obtained from the MD simulations of the left- and right-wound Py₇ oligomers. Here only the antiparallel relative orientation of the dipoles was considered (see the Results section). The C nucleotide was linked at the end of the

Py₇ oligomer through the phosphorus atom. The valence of the O3'@C atom was saturated adding one hydrogen atom to it.

Py₇/Py₇ complexes were studied using six representative self-assembly possibilities, named 2Py₇^{*i*}, where *i* indicate the number of pyrenes of each individual Py₇ filament intercalated into the other one. The procedure for building the starting guess structures of the complexes was analogous to the one followed for the single oligomers. Specifically, we first packed the pyrenes belonging to the *intercalation domain*, that is, the region characterized by the intercalated units. Then, we reconstructed the linker groups in this region. Finally, we added the external portions (*single oligomer domains*) of the two Py₇ molecules. Structural information obtained from the single Py₇ simulations were used to build the guess structures of the complexes in these peripheral *single oligomer domains*. Py₇-C/Py₇ structures were built exploiting the structural information obtained for 2Py₇³, carefully inserting the C nucleotide into the pyrene stacking region.

The stretching, bending, and torsional parameters for the pyrene monomers were taken from the GAFF force field.⁴⁹ Atomic point charges were calculated for the single pyrene unit using the well established RESP procedure.^{50,51} An appropriate number of Na⁺ counterions was added to achieve electro-neutrality to each simulated system. An additional 160 Na⁺ and Cl[−] ion pairs were added to mimic the experimental 1 M NaCl concentration conditions.²⁷ The systems were solvated by addition of a shell of TIP3P water molecules,⁵² initially randomly distributed in the simulation box, with a radius of 18 Å from the solute and put in orthorhombic periodic boxes of 90 × 95 × 100 Å³. NPT conditions were applied using a Nosé–Hoover Langevin barostat^{53,54} and Langevin thermostat.⁵⁵ The SHAKE algorithm⁵⁶ was used to treat all bonds involving hydrogens. Equations of motions were solved using the velocity Verlet algorithm,^{57,58} with a time step of 1.5 fs. Initially, 2 ns of simulations were run to bring and equilibrate the system to room temperature, and pressure conditions, followed for 100 ns of production.

The MD trajectories were generated with the NAMD software,⁵⁵ while all analyses were performed with the VMD software.⁵⁹

Free Energy Estimations. The free energies of all 2Py₇^{*i*} models were calculated using the well established thermodynamic cycle between two separated heptapyrenotides and its assembly, as in refs 60–62. Within this approach, the difference in the binding free energy between two 2Py₇^{*i*}–2Py₇^{*j*} complexes is given by the difference of the respective solvation energies, plus the difference of the internal energy and entropy contribution in vacuo.

Solvation energies were obtained by solving the linearized Poisson–Boltzmann equation for the 2Py₇^{*i*} complexes using values of the dielectric constants of 78 and 1 to mimic the dielectric response of water and vacuo, respectively. All calculations were performed with the APBS software.⁶⁰ The force field energy was used to estimate the binding energy *in vacuo*. Entropy contributions in vacuo were estimated by statistical mechanics and analysis of the normal modes, as implemented in the Amber MMPBSA module,^{63,64} for three complexes (2Py₇^{*i*} with *i* = 1, 3, and 5). In all complexes, the difference of entropy resulted in being smaller than the statistical uncertainty ($\Delta\Delta S = 1 \pm 3$ kJ mol^{−1}); therefore, we did not consider it any further in our study. All quantities were averaged over a set of 2000 independent structures sampled randomly along the equilibrated MD runs.

RESULTS

QM Calculations. The preference for π – π stacking geometries in pyrene aggregates has already been well determined in the literature (see as an example refs 36, 65, and 66). The presence of such a conformation among pyrenes in the heptapyrenotides has also been confirmed by previous UV/vis and fluorescence spectroscopy measurements.⁹ The 1,8-position of the covalent linkers attached to the pyrene ring breaks the symmetry of the molecule. Given the polarity of the carboxamide groups covalently bound to the pyrene moiety, a neat electrostatic dipole is formed (Figure 1C). In our preliminary QM calculations, we repeated geometry optimizations using as initial guess conformations the two limit cases: the first with the two pyrenes having parallel electrostatic dipoles, and the second with pyrenes having antiparallel dipoles. We found that only the antiparallel arrangement formed stable stacking dimers, while the parallel geometry did not converge to a minimum energy structure. In fact, the antiparallel orientation converged to a structure where the pyrenes arranged in a π – π stacking conformation, with an interplanar distance of 3.5 Å, in agreement with the stacking distances of pyrene systems previously published.^{36,65,66} On the contrary, when starting from the in parallel orientation of the two dipoles, the structure resulted in being highly unstable, with the pyrene groups moving apart from each other, thus losing the expected stacking conformation.

MD of Single Heptapyrenotide. Py₇ with Antiparallel Dipole Moments. The system was relaxed with MD for 2 ns; then, a production run of 100 ns was performed. The RMSD evolution plot (Figure 1, Supporting Information), calculated on the carbon atoms of the pyrenes and of the linkers, shows that the starting structure relaxed quickly in ~ 1 ns to a geometry with a RMSD value of ~ 6 Å from the initial one. After this initial large structural relaxation, the structure of Py₇ found a new, stable conformation, characterized by a relative RMSD smaller than 1 Å for the rest of the simulated time. The relaxed structure shows some striking structural features vaguely recalling those of DNA filaments. First, our oligomer keeps a global cylindrical shape, with a height of ~ 24 Å and a diameter of ~ 20 Å. Second, the pyrenes maintain a π – π stacking conformation, with an average interplane distance between two consecutive pyrenes of 3.6 ± 0.1 Å. The longitudinal axes of two consecutive pyrenes result in being twisted by about 30° (Figure 3C).

This very regular twisting of the stacking groups defines a precise helical structural motif (Figure 4). As the pyrene units are assembled in an antiparallel orientation, the corresponding twist angle between dipole moments associated with consecutive pyrene units is complementary and opposite in sign to the twisting angle between the pyrene axes (-150°) (Figure 3C). That is, the electrostatic dipoles of the pyrenes rotate opposite to the helical groove.

Given the absence of any chiral centers in the covalent chemical structure of the polymer, it is expected that the specular enantiomeric superstructure has the same statistical probability of being formed. In fact, starting a different MD run from the specular symmetric geometry of our arbitrarily chosen initial structure, and repeating the same procedure described for our first calculation, the structure developed systematically into the same kind of helix but with the opposite chirality (Figure 4).

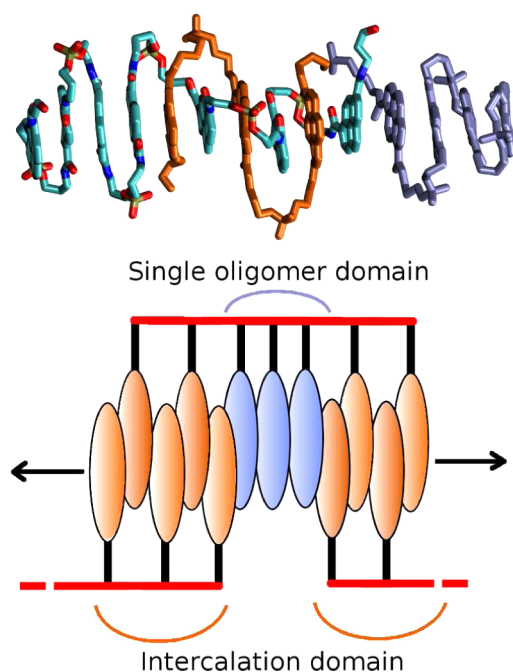


Figure 2. Schematic representation of supramolecular oligomerization. The supramolecular fibril is characterized by alternation of *intercalation domains* and *single oligomer domains*.

The formation and stability of this helical structure is induced by peculiar interactions occurring at the linker. Specifically, we observe the formation of very stable H-bonds between the NH donor groups of the two amide moieties connecting two consecutive pyrenes and the phosphate group connecting them (Figure 3A). These H-bonds form during the folding into the helical structure and, apart from instantaneous fluctuations, remain for the whole length of the simulation. The twist of two consecutive pyrenes is therefore associated with this particularly stable folding of the linker. We also note that the twisting of the pyrenes consistently increases the angular distance between phosphate groups, thus minimizing the destabilizing charge–repulsion interactions. In particular, the six phosphates arranged uniformly in the space around the elongation axis during the simulation, spanning almost a complete turn, resembling the winding staircase structure of the nucleic acids (Figure 4).

A general helical folding is expected for optimal packing of rod-like objects with a hydrophobic core that must be screened from polar solvents.⁶⁷ In fact, the peculiar conformation of the

linker screens the sides of the aromatic hydrophobic core of the oligomer, resulting in formation of two symmetric grooves sculpted according to the winding rotation of the system. The surface of each groove is created by the solvent exposed, long edge part of the pyrene rings, while its boundary is defined by the corrugation created by the winding linkers (Figure 4). In such a relaxed conformation, the solvent accessible surface area (SASA) of the helix is $\sim 200 \text{ \AA}^2$ smaller than in the initial starting structure.

Analysis of the structure of the water in the proximity of the pyrenes shows a spontaneous organization of a hydrogen-bond network of three water molecules at each pyrene plan. These are involved in a well-defined hydrogen bond network, two of them donating H-bonds to the carboxyl groups of the linkers and a third water molecule creating a bridge with the former two (Figure 5). The very regular organization of this water network is stabilized by the optimal alignment of the electrostatic dipole of the bridging water with one of the corresponding pyrenes.

Py₇ with Parallel Dipole Moments. Another starting configuration was also considered for Py₇, where the electrostatic dipoles associated with each pyrene were arranged in parallel. Though our QM *in vacuo* calculations predict strong instability for this particular packing conformation, we went through these simulations to evaluate any possible stabilization due to hydrophobic effects coming from pyrene–pyrene packing in a highly polar solvent like water. In fact, in the relatively short simulation time (100 ns), the pyrene units do not lose their local stacking geometry. This was expected, as direct exposure of the pyrenes to water would lead to too strongly unfavored conformations. Nonetheless, the global structure of the assembly results in being strongly distorted and does not show the same optimal packing as observed in the antiparallel model. In fact, the total solvent accessible surface area does not significantly decrease from that of the initial structure, unlike in the antiparallel stacking.

In the parallel assembly, the amide linker groups face all the same sides of the oligomer. As a result, the two grooves of the helix are strongly asymmetric, one being characterized by a strong hydrophobic character, while the other bringing all hydrophilic amide groups. This eventually leads to a distorted assembly of the whole heptapyrenotide, which shows an irregular kink along its longitudinal axis. This is particularly significant, as AFM images have shown how these oligomers can consistently keep their longitudinal directionality for several nanometers.²⁷ Finally, the pyrene linkers do not show the

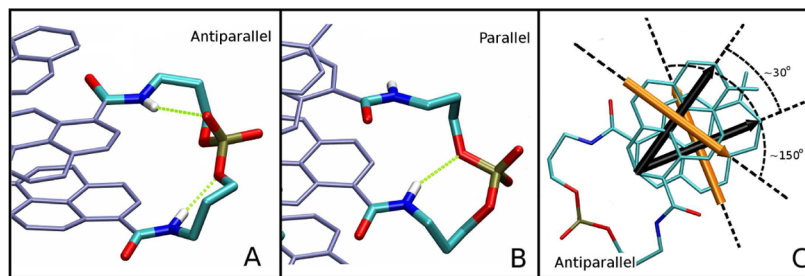


Figure 3. Organization of the linker group and twisting angle of consecutive pyrene groups in Py₇. (A) Organization of the linker when there is a consecutive pyrene stack in antiparallel geometry. The intramolecular hydrogen bonds are highlighted by dotted green lines. (B) Organization of the linker when there is a consecutive pyrene stack in parallel geometry. (C) Top view of the arrangement of two consecutive pyrene units in antiparallel stacking. The black arrows indicate the long axis of the pyrenes, and the orange arrows show the orientation of the corresponding molecular electrostatic dipoles.

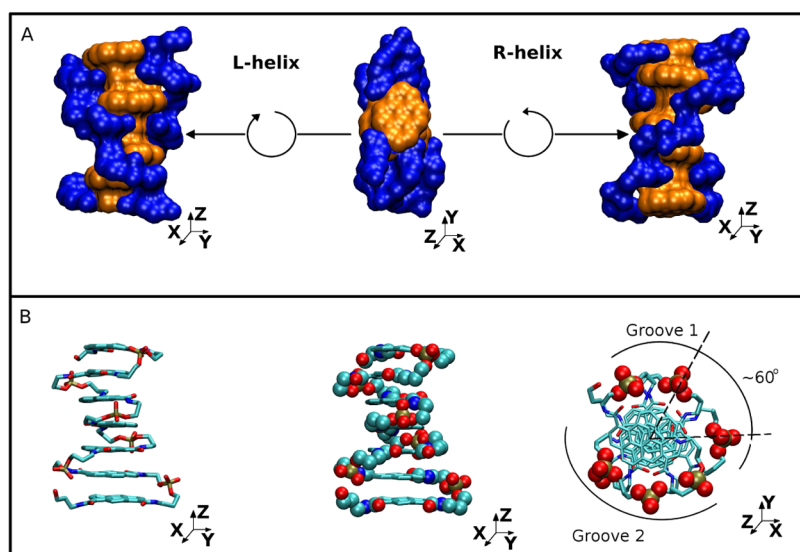


Figure 4. Helical structures of Py_7 . (A) In the middle, the initial guess structure is shown, while the relaxed left-wound and right-wound helices, as found by MD simulations, are shown on its left and right, respectively. The pyrene units are represented by an orange surface, the linkers, by a blue surface. (B) Atomistic top-view representation of the relaxed Py_7 . The symmetric distribution of the phosphate groups of the linkers (outlined as a VdW sphere) is highlighted by dashed black lines.

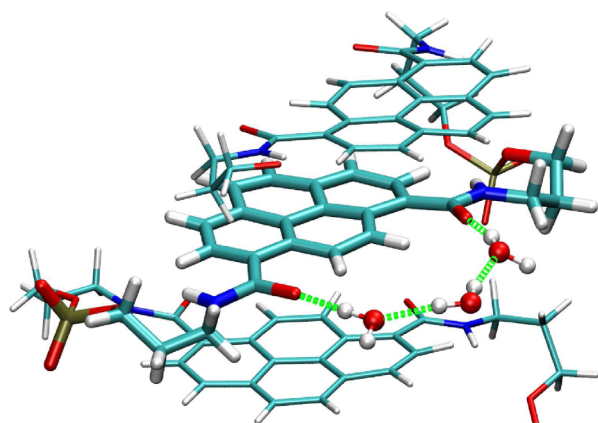


Figure 5. Hydration of pyrene units in the groove. One pyrene unit and the amide groups covalently bonded to it are represented in licorice. Stacking pyrenes are represented in thin licorice. The three water molecules constituting an organized H-bond network in the groove are drawn in balls-and-sticks. The hydrogen bonds are highlighted by dashed green lines.

regular H-bond assembly present in the antiparallel configuration. In particular, our MD run data show that, in this case, the phosphate groups are able to form only one H-bond with

the adjacent amide moieties (Figure 3A). Therefore, linker groups result in being overall less stabilized by H-bonding than in the antiparallel assembly.

As the parallel stacking conformation results are less favorable with respect to the antiparallel one, they were not further considered in our study.

$\text{Py}_7\text{-C}$. The models for the $\text{Py}_7\text{-C}$ were prepared starting from the final relaxed structure obtained from the MD simulations of the left- and right-wound antiparallel model of Py_7 oligomers. The initial conformation was designed so that both the sugar and the nucleobase of C were fully hydrated, forming minimal non-covalent contacts with the rest of the polymer. During our simulations, the C nucleobase has a very fast displacement to its relaxed position, which has an average RMSD from the initial configuration of ~ 2 Å.

In the relaxed structure, the NH group of the linker amide which connects Py_7 to the nucleotide is involved in H-bond contacts with the oxygens of the phosphate group of C (80% of the simulated time), and with the O4' oxygen of the ribose (20%). The OH group of the sugar is always forming weak H-bonds with the neighboring solvent water molecules.

The pyrimidine ring of C lies in proximity to the terminal pyrene in the oligomer chain, with which it interacts by π - π stacking (Figure 6). The different size between the nucleobase and the pyrene allows for different optimal stacking geometries,

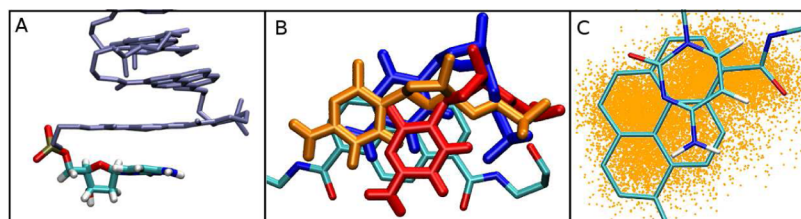


Figure 6. Organization of $\text{Py}_7\text{-C}$. (A) Side view of the relaxed geometry of C in a single $\text{Py}_7\text{-C}$ unit. Py_7 is represented in ice-blue thin licorice, C in licorice, and colored using standard atom-color code. (B) Top view of the stacking interaction between Py_7 and C. Three representative conformations of C are represented in blue, red, and orange licorice. (C) Statistical distribution of the (x, y) position of the center of mass of C with respect to the corresponding stacking pyrene. Each orange dot represents one conformation from our MD simulation.

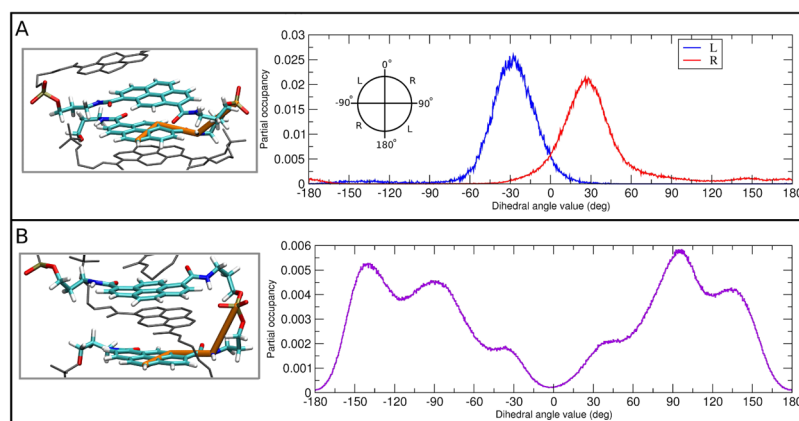


Figure 7. Folding of the linkers in Py_7 and 2Py_7^i . The spatial displacement of the linkers was monitored considering the dihedral angle represented in orange licorice on the left part of the picture. (A) The distribution of the value in Py_7 and in the *single oligomer domain* for the R-wound (red line) or L-wound helix (blue line). (B) The distribution of the same dihedral angle in the *intercalation domain*.

where the single aromatic ring of C pairs to one of the condensed rings of pyrene proximal to the side where the sugar is localized (Figure 6).

In fact, we find high root-mean-square fluctuation values for the pyrimidine ring of C, corresponding to the displacement of the nucleobase between multiple stacking positions (Figure 6 and Table 1, Supporting Information). As C interacts weakly and aspecifically with Py_7 , it does not influence the global assembly of it. In fact, in our simulations, we find that the global arrangement of the pyrene units and linkers is not affected by the presence of C, and it remains very similar to what was found in Py_7 . Therefore, our model predicts no selection of the left- or right-wound helical arrangement in $\text{Py}_7\text{-C}$, and thus a racemic mixture of the two is expected, consistent with the experimental CD measurements, which do not show any chiral signal for a solution of $\text{Py}_7\text{-C}$ oligomers.⁹

Heptapyrenotide Self-Assembly. 2Py_7^i . At the experimental level, very little is known about the structure and formation kinetics of non-covalent assemblies of heptapyrenotides. AFM measurements confirm the formation of filaments with a thickness compatible with the dimension of single-stacked pyrene chains.³⁵ Therefore, it is reasonable to guess that the formation of fibrils occurs through longitudinal extension of the oligomers. As already suggested in refs 9 and 27, intercalation of pyrenes coming from different single chains is expected to occur, but the average number of pyrenes involved in these inter-oligomer organizations is not known.

Assuming that polymerization occurs by pyrene intercalation, as also confirmed by recent AFM data,³⁵ the structure of a self-assembled fibril can be divided into different domains: (i) regions of the fibril where pyrenes, belonging to distinct heptapyrenotides, are involved in inter-oligomer stacking interactions (*intercalation domains*); (ii) regions where the pyrenes belonging to the same single heptapyrenotide strands assemble independently, therefore resembling single Py_7 (*single oligomer domains*).

Intercalation Domain: Structural Features. In MD simulations of the different Py_7^i complexes, all structures maintain a regular cylindrical shape, with a diameter of ~ 22 Å. The π - π stacking among pyrenes is also kept, with an average pyrene separation of 3.6 ± 0.1 Å.

Figure 7 displays the geometry of the linker connecting two pyrenes intercalated by another one from a different Py_7 monomer in a generic Py_7^i assembly. The elongated interplanar

distance between two linked pyrenes requires the amide-phosphate moieties adopt an almost fully extended geometry.

In fact, given the shortness of the linking phosphate-dipyrenotide moiety, only one pyrene from one Py_7 oligomer can be accommodated between two pyrenes of the other Py_7 oligomer (Figure 7) without accumulation of excessive strain in the structure. While connecting intercalated pyrenes, no intralinker H-bonds can be formed. As a result, the phosphate group remains fully exposed to the solvent. The complete lack of H-bond interactions in the *intercalation domain* gives some conformational freedom to the structure. As a consequence of such increased mobility, the pyrene rings slightly modify their relative orientation, losing the perfect antiparallel organization imposed in the starting structure.

The orientation of the linkers, which in the starting guess was parallel to the axis of elongation, changes during the MD production, distributing around two conformations (Figure 7).

The phosphates, pushed by the electrostatic repulsion which arises among them, increase their relative distance and spread uniformly in the space.

The slight increase in the first peak value of the pair correlation function of the water oxygens from the phosphate atoms in the *intercalation domain* (see Figure 3, Supporting Information) shows that the phosphate groups in this linker conformation lay more solvent exposed and interact more strongly with the water. On the contrary, the solvation pattern close to the polar side of the pyrenes is very similar to what was observed for the single heptapyrenotide models, and at each pyrene plane, three water molecules form the same H-bond network as previously described.

In order to estimate the relative probabilities for the formation of the different Py_7^i complexes, we estimated the relative free energies for these systems averaging results over 2000 uncorrelated structures sampled from our MD runs. We find that intercalation of each pyrene unit corresponds to an average increase of the free energy of about 5.9 ± 2 kJ/mol. Therefore, our estimates suggest that, in solution, different Py_7^i conformations are present. In any case, the species with a majority of pyrenes not participating in the intermolecular interactions are thermodynamically more stable, and therefore are supposed to be statistically the most abundant.

Symmetry Breaking in $\text{Py}_7\text{-C}/\text{Py}_7$. Assemblies obtained from stoichiometric 1:1 mixtures of $\text{Py}_7\text{-C}/\text{Py}_7$ oligomers have shown to give a strong CD signal, indicating emergence of

assembled species with a well determined chirality.²⁷ The selection of a chiral structure upon asymmetric $\text{Py}_7\text{-C}/\text{Py}_7$ self-assembly formation can be rationalized by taking into account possible interactions between the chiral, helical supramolecular assembly of the polymer and the chiral moiety covalently bound to the $\text{Py}_7\text{-C}$ isoform, namely, the sugar of C.

As previously discussed for the single $\text{Py}_7\text{-C}$ model, the C nucleotide is not able to induce any chirality into the system, when it interacts with the terminal part of the assembled supramolecular complex.

In order to address the effect induced by the presence of the C nucleotide in 2Py_7^i complexes, two starting conformations were built from the structure obtained in 2Py_7^i , with the aromatic moiety of C stacked between the last pyrene in the *intercalation domain* and the first one in the *single oligomer domain*.

Specifically, the *single oligomer domains* were arranged in the left- and right-wound helix, so that both possible chiralities were considered. In both chiral models, the pyrimidine was expelled from the aromatic core formed by the pyrenes in less than 1 ns, and after that, it interacted with the external edge of the system and with the solvent. This can be expected, given the smaller size of the aromatic portion of C with respect to the pyrenes. Moreover, C is significantly more hydrophilic than the pyrene units. Apart from that, both the *intercalation domain* and the *single oligomer domain* maintained all the structural and dynamical features previously described in the 2Py_7^i assemblies and in the Py_7 monomer, respectively.

On the contrary, C showed a striking different behavior in the two chiral models considered. In the first nanosecond after extrusion, in both systems, C mostly interacted with the solvent, forming only transient contacts with the groove of the helix. This was maintained for the whole length of the simulation of the right-wound system. In particular, the position of C was not clearly defined, as it formed nonspecific interactions with the solvent, the *intercalation domain*, or the *single oligomer domain*, all of them being characterized by relatively short residence times of less than 20 ns.

In the left-wound system instead, after the extrusion from the aromatic core, the C nucleotide showed a very clear affinity for the neighboring *single oligomer domain*, which was approached within 2–4 ns. After formation of the initial contacts, dominated mostly by T-shape dispersion interactions between the pyrene and the pyrimidine, the localization of C at the *single oligomer domain* was further stabilized by a H-bond between the hydroxyl group of the sugar of the nucleotide and the carbonyl group of the adjacent pyrene. The progressive formation of this very stable H-bond, which apart from local thermal fluctuations was never broken throughout the rest of the 100 ns of the MD simulation, is shown in Figure 8. After H-bond formation, both the sugar and the aromatic moieties of C accommodate in the groove of the helix, thanks to an optimal shape complementarity (Figure 8C).

The simultaneous presence of stabilizing hydrogen bonds and hydrophobic contacts was never seen in the model with opposite chirality of the helix, as formation of any H-bond between the sugar and the linker corresponded to nonoptimal configurations for the base, characterized by either steric clashes with the groove or resulting in highly solvated geometries. The different stabilization of the geometry of C can be evidenced by the continuous changes in the dihedral angle of linker atoms (Figure 4, Supporting Information), to which multiple changes correspond in the position of the sugar.

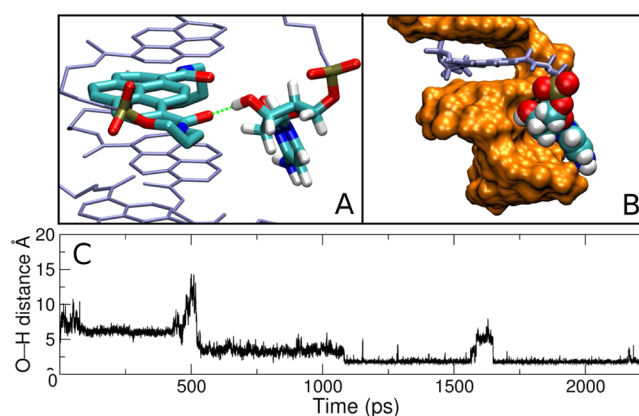


Figure 8. Interaction of C with the left-wound groove of Py_7 . (A) The H-bond between the OH group of ribose of C with the CO group of the adjacent pyrene is shown. (B) Formation of the H-bond shown in panel A as a function of time. The O...H distance is reported. (C) Shape complementarity between the C nucleotide and the left-wound groove of Py_7 . Py_7 is represented by its surface, colored in orange, and C is represented in van der Waals spheres.

DISCUSSION

Despite the wealth of experimental data produced,^{27–29} which allowed for understanding of the physicochemical characteristics of the Py_7 polymer, the lack of a detailed molecular structure for neither its monomeric nor its superassembled states hinders the possibility of further developing the design and synthesis of specifically functionalized chemical variants. Given the difficulties in resolving experimentally the structure of Py_7 , we built here a series of computational models that turned out to be fully consistent with the experimental observations available. Our models show that monomeric units of Py_7 can fold in well structured helices. The driving force for such packing is provided by the hydrophobic collapse of the pyrene units in the central core of stacked aromatic planes. The most energetically favorable packing of the pyrene units is the one in which the electric dipoles associated with each pyrene displace in an almost antiparallel direction with respect to those in the neighboring planes. This peculiar packing is also stabilized by the organization of the linkers, which assemble in an intramolecular H-bond network connecting the two amide moieties and the phosphate groups belonging to the same linking unit. This very well structured intramolecular assembly defines with good precision the twisting angle of the helix, which corresponds to roughly 30° at each pyrene plane.

This finding opens to the design of selective modifications of the linkers able to assemble in different organizations, thus yielding helices with different twisting angles. The possibility of modulating the twisting between consecutive stacking units can be of use, for example, for the synthesis of Py_7 -like systems with tailored optical properties at specific sites of the sequence.

Experimental imaging and AFM measurements^{27,35} revealed that Py_7 is able to polymerize by π stacking and pyrene interstrand intercalation, forming linear high-molecular-weight multimers. AFM imaging suggests that these units have a transversal dimensionality similar to that found in our simulations (20 Å for monomers and 22 Å for dimers). Therefore, we can assume that supramolecular polymerization occurs along the longitudinal direction only. We have tested different possible intercalation geometries, and estimated the

binding free energy differences for them. Our calculations reveal that, given the short molecular length of the linker, not more than one pyrene of one Py_7 unit can intercalate between two pyrenes of the second strand. Moreover, the free-energy cost of intercalating each pyrene unit is such that only a minor portion of the pyrenes probably intercalate. Hence, our models support the view that, in the supramolecular organization, Py_7 units assemble by intercalating only part of their pyrenes. Therefore, it is likely that a $n\text{Py}_7$ fibril alternates regions of interactions where pyrenes from two units are intercalated to regions where pyrenes from one single oligomer stack in a monomer-like (i.e., single-stranded) organization (Figure 2).

The hypothesis that a full intercalation between monomeric units does not happen in solution also has a kinetic rationale. In fact, in order to intercalate respecting the *antiparallel* alternation, pyrenes must swap face. Therefore, it is reasonable to think that reactive collisions between Py_7 units imply intercalation of a few units only. We expect that intercalation is facilitated by local fluctuations of the structure from its equilibrium geometry. In fact, in our simulations, we find a higher mobility of the pyrene units at the ends of Py_7 than the ones in the core of the molecule (Table 1, Supporting Information). This again hints at 2Py_7^i species with low values of i to be those that are formed with higher probability. Experimental evidence points at the ionic strength as a key factor for the stabilization of the π -stacked assemblies in Py_7 . Unfortunately, given the polyanionic nature of the oligomers under study, and the necessity of treating the molecular nature of the solvent explicitly to get accurate results, we could not reduce the ionic strength in our simulations below thresholds that would eventually lead to loss of ordered structures, as this could have been reached only by increasing the simulation box to dimensions too large for feasible computational costs. The strong correlation between the linker structure and the solvated ions can be evidenced by computing the radial distribution function between the phosphate atoms and the Na^+ ions. In fact, these plots show at least three clear solvation structures before the bulk (Figure 2, Supporting Information), with 9 Na in the first shell.

The accumulation of ions around the phosphate at the *intercalation domain* must be attributed to the absence of the shielding effects by the amide units, present in the folded *single oligomer domain* and in Py_7 structures.

One of the most puzzling experimental findings in Py_7 research has been the evidence of chirality enhancements upon supramolecular complexation of asymmetric $\text{Py}_7\text{-C}/\text{Py}_7$ units. Our simulations show that the simple attachment of a single C nucleotide to the Py_7 strand is not able to induce a specific chirality to the monomeric assembly. Therefore, like in normal Py_7 , a 1:1 mixture of both helical windings is expected. On the contrary, interaction of C at the intercalation region of intercalating dimers is significantly different for left-wound or right-wound helices. In particular, we find that C has a striking shape complementarity with the left-wound helix. During our MD simulations, we observe localization of C in a niche of the groove. The conformation of C in the groove is further stabilized by the formation of a highly resilient H-bond between the hydroxyl group of its sugar and one amide carbonyl of the neighboring linker group. Therefore, our MD simulations suggest that the mechanism of chirality enhancement passes through a *lock-in* interaction of the C base with the groove. This peculiar interaction resembles that of specific drugs designed to recognize and bind to the DNA grooves (see, i.e., refs 68–71),

which are meant to modify the structural and dynamical features of the target supramolecular assembly. In this view, our structures suggest the possibility of designing specific molecules with high affinity for the different grooves, able to dynamically and reversibly modulate the relative ratio of the racemic mixture for these assemblies.

Our simulations show how the left-wound arrangement is favored by the presence of C. For symmetry reasons, the left wound rotation of the structure corresponds to a right-wound rotation of the electronic orbitals of the stacked pyrenes, which are responsible for the signal collected in the CD spectrum. This confirms the modulation of the chirality signal published in refs 9 and 27 which was qualitatively interpreted as a fingerprint for formation of a DNA-like right-wound helix.

CONCLUSIONS

Through a series of calculations, we have elucidated the structure of single and assembled heptapyrenotide molecules, alone or with an additional C nucleotide attached to them. From our results, we are able to provide a rational explanation on the emergence of chirality under particular experimental conditions, specifically high salt concentration, where fibrils with a specific chirality are expected to form. Our calculations show that single chains arrange in structured helices of well-defined chirality. The formation of supramolecular polymers is supported by intercalative interactions between pyrenes of different strands. The presence of a C nucleobase at the terminal part of the single heptapyrenotides is able to select the left-wound chirality by optimal shape complementarity and by formation of a stable H-bond of the 3'-hydroxyl with the amide linker. While corroborating the previous conclusions drawn from spectroscopic experiments, these calculations also provide a rational basis for the further development of oligopyrenotide-derived supramolecular materials.

ASSOCIATED CONTENT

Supporting Information

Table and graphs reporting the following: RMSD and RMSF of Py_7 and $\text{Py}_7\text{-C}$; radial distribution function of P-Na^+ and $\text{P-O@H}_2\text{O}$; linker fluctuations at C of $\text{Py}_7\text{-C}$ interacting with a left- or right-wound helix. This material is available free of charge via the Internet at <http://pubs.acs.org>.

AUTHOR INFORMATION

Corresponding Author

*E-mail: michele.casella@iac.unibe.ch. Phone: +41 31 631 4256.

Notes

The authors declare no competing financial interest.

ACKNOWLEDGMENTS

This research was supported by the Swiss National Science Foundation (Grants NN. PP02-118930 and PP00P2_139195 for M.C.; Grant 200020_132581 for R.H.).

REFERENCES

- (1) Aida, T.; Meijer, E. W.; Stupp, S. I. Functional Supramolecular Polymers. *Science* **2012**, 335, 813–817.
- (2) Korevaar, P. A.; George, S. J.; Markvoort, A. J.; Smulders, M. M.; Hilbers, P. A.; Schenning, A. P.; De Greef, T. F.; Meijer, E. W. Pathway Complexity in Supramolecular Polymerization. *Nature* **2012**, 481, 492–496.

- (3) Palmer, L. C.; Stupp, S. I. Molecular Self-Assembly into One-Dimensional Nanostructures. *Acc. Chem. Res.* **2008**, *41*, 1674–1684.
- (4) Brunsveld, L.; Folmer, B. J. B.; Meijer, E. W.; Sijbesma, R. P. Supramolecular Polymers. *Chem. Rev.* **2001**, *101*, 4071–4098.
- (5) Lehn, J.-M. Supramolecular Polymer Chemistry – Scope and Perspectives. *Polym. Int.* **2002**, *51*, 825–839.
- (6) Moore, J. S. Supramolecular Polymers. *Curr. Opin. Colloid Interface Sci.* **1999**, *4*, 108–116.
- (7) Saenger, W. *Principles of Nucleic Acid Structure*; Springer-Verlag: New York, 1984.
- (8) *Oxford Handbook of Nucleic Acid Structure*; Oxford University Press: New York, 1999.
- (9) Albrecht, M. Artificial Molecular Double-Stranded Helices. *Angew. Chem., Int. Ed.* **2005**, *44*, 6448–6451.
- (10) Nielsen, P. E.; Haaima, G. Peptide Nucleic Acid (PNA). A DNA Mimic with a Pseudopeptide Backbone. *Chem. Soc. Rev.* **1997**, *26*, 73–78.
- (11) Eschenmoser, A. Chemical Etiology of Nucleic Acid Structure. *Science* **1999**, *284*, 2118–2124.
- (12) Herdewijn, P. Conformationally Restricted Carbohydrate-Modified Nucleic Acids and Antisense Technology. *Biochim. Biophys. Acta* **1999**, *1489*, 167–179.
- (13) Wengel, J. Synthesis of 3'-C- and 4'-C-Branched Oligodeoxynucleotides and the Development of Locked Nucleic Acid (LNA). *Acc. Chem. Res.* **1999**, *32*, 301–310.
- (14) Kool, E. T. Preorganization of DNA: Design Principles for Improving Nucleic Acid Recognition by Synthetic Oligonucleotides. *Chem. Rev.* **1997**, *97*, 1473–1488.
- (15) Teo, Y. N.; Kool, E. T. DNA-Multichromophore Systems. *Chem. Rev.* **2012**, *112*, 4221–4245.
- (16) Malinovskii, V. L.; Wenger, D.; Häner, R. Nucleic Acid-Guided Assembly of Aromatic Chromophores. *Chem. Soc. Rev.* **2010**, *39*, 410–422.
- (17) Seeman, N. C. Nanomaterials Based on DNA. *Annu. Rev. Biochem.* **2010**, *79*, 65–87.
- (18) McLaughlin, C. K.; Hamblin, G. D.; Sleiman, H. F. Supramolecular DNA Assembly. *Chem. Soc. Rev.* **2011**, *40*, 5647–5656.
- (19) Heckel, A.; Famulok, M. Building Objects from Nucleic Acids for a Nanometer World. *Biochimie* **2008**, *90*, 1096–1107.
- (20) Sherrington, D. C.; Taskinen, K. A. Self-Assembly in Synthetic Macromolecular Systems via Multiple Hydrogen Bonding Interactions. *Chem. Soc. Rev.* **2001**, *30*, 83–93.
- (21) Schmuck, C.; Wienand, W. Self-Complementary Quadruple Hydrogen-Bonding Motifs as a Functional Principle: From Dimeric Supramolecules to Supramolecular Polymers. *Angew. Chem., Int. Ed.* **2001**, *40*, 4363–4369.
- (22) Prins, L.; Reinhoudt, D.; Timmerman, P. Noncovalent Synthesis Using Hydrogen Bonding. *Angew. Chem., Int. Ed.* **2001**, *40*, 2382–2426.
- (23) Wilson, A. J. Non-Covalent Polymer Assembly Using Arrays of Hydrogen-Bonds. *Soft Matter* **2007**, *3*, 409–425.
- (24) Huc, I. Aromatic Oligoamide Foldamers. *Eur. J. Org. Chem.* **2004**, *2004*, 17–29.
- (25) Meyer, E. A.; Castellano, R. K.; Diederich, F. Interactions with Aromatic Rings in Chemical and Biological Recognition. *Angew. Chem., Int. Ed.* **2003**, *42*, 1210–1250.
- (26) Häner, R.; Garo, F.; Wenger, D.; Malinovskii, V. L. Oligopyrenotides: Abiotic, Polyanionic Oligomers with Nucleic Acid-like Structural Properties. *J. Am. Chem. Soc.* **2010**, *132*, 7466–7471.
- (27) Nussbaumer, A. L.; Studer, D.; Malinovskii, V. L.; Häner, R. Amplification of Chirality by Supramolecular Polymerization of Pyrene Oligomers. *Angew. Chem., Int. Ed.* **2011**, *50*, 5490–5494.
- (28) Nussbaumer, A. L.; Samain, F.; Malinovskii, V. L.; Häner, R. Supramolecular Polymerization of Oligopyrenotides – Control by Single, Natural Nucleotides. *Org. Biomol. Chem.* **2012**, *10*, 4891–4898.
- (29) Malinovskii, V. L.; Nussbaumer, A. L.; Häner, R. Oligopyrenotides: Chiral Nanoscale Templates for Chromophore Assembly. *Angew. Chem., Int. Ed.* **2012**, *51*, 4905–4908.
- (30) Oosawa, F.; Kasai, M. A Theory of Linear and Helical Aggregations of Macromolecules. *J. Mol. Biol.* **1962**, *4*, 10–21.
- (31) Martin, R. B. Comparisons of Indefinite Self-Association Models. *Chem. Rev.* **1996**, *96*, 3043–3064.
- (32) Zhao, D. H.; Moore, J. S. Nucleation-Elongation: a Mechanism for Cooperative Supramolecular Polymerization. *Org. Biomol. Chem.* **2003**, *1*, 3471–3491.
- (33) Smulders, M. M. J.; Nieuwenhuizen, M. M. L.; de Greef, T. F. A.; van der Schoot, P.; Schenning, A. P. H. J.; Meijer, E. W. How to Distinguish Isodesmic from Cooperative Supramolecular Polymerisation. *Chem.—Eur. J.* **2010**, *16*, 362–367.
- (34) Korevaar, P. A.; Schaefer, C.; de Greef, T. F. A.; Meijer, E. W. Controlling Chemical Self-Assembly by Solvent-Dependent Dynamics. *J. Am. Chem. Soc.* **2012**, *134*, 13482–13491.
- (35) Rudnev, A. V.; Malinovskii, V. L.; Nussbaumer, A. L.; Mishchenko, A.; Häner, R.; Wandlowski, T. Cooperative and Noncooperative Assembly of Oligopyrenotides Resolved by Atomic Force Microscopy. *Macromolecules* **2012**, *45*, 5986–5992.
- (36) Podeszwa, R.; Szalewicz, K. Physical Origins of Interactions in Dimers of Polycyclic Aromatic Hydrocarbons. *Phys. Chem. Chem. Phys.* **2008**, *10*, 2735–2746.
- (37) Becke, A. D. Density-Functional Exchange-Energy Approximation With Correct Asymptotic Behavior. *Phys. Rev. A* **1988**, *38*, 3098–3100.
- (38) Lee, C.; Yang, W.; Parr, R. G. Development of the Colle-Salvetti Correlation-Energy Formula into a Functional of the Electron Density. *Phys. Rev. B* **1988**, *37*, 785–789.
- (39) Miehlich, B.; Savin, A.; Stoll, H.; Preuss, H. Results Obtained with the Correlation Energy Density Functionals of Becke and Lee, Yang and Parr. *Chem. Phys. Lett.* **1989**, *157*, 200–206.
- (40) Goedecker, S.; Teter, M.; Hutter, J. Separable Dual-Space Gaussian Pseudopotentials. *Phys. Rev. B* **1996**, *54*, 1703–1710.
- (41) Hartwigsen, C.; Goedecker, S.; Hutter, J. Relativistic Separable Dual-Space Gaussian Pseudopotentials from H to Rn. *Phys. Rev. B* **1998**, *58*, 3641–3662.
- (42) Krack, M. Pseudopotentials for H to Kr Optimized for Gradient-Corrected Exchange-Correlation Functionals. *Theor. Chem. Acc.* **2005**, *114*, 145–152.
- (43) von Lilienfeld, O. A.; Tavernelli, I.; Rothlisberger, U.; Sebastiani, D. Optimization of Effective Atom Centered Potentials for London Dispersion Forces in Density Functional Theory. *Phys. Rev. Lett.* **2004**, *93*, 153004.
- (44) Lin, I. C.; Coutinho-Neto, M. D.; Felsenheimer, C.; von Lilienfeld, O. A.; Tavernelli, I.; Rothlisberger, U. Library of Dispersion-Corrected Atom-Centered Potentials for Generalized Gradient Approximation Functionals: Elements H, C, N, O, He, Ne, Ar, and Kr. *Phys. Rev. B* **2007**, *75*, 205131.
- (45) Cascella, M.; Lin, I. C.; Tavernelli, I.; Rothlisberger, U. Dispersion Corrected Atom-Centered Potentials for Phosphorus. *J. Chem. Theory Comput.* **2009**, *5*, 2930–2934.
- (46) Martyna, G. J.; Tuckerman, M. E. A Reciprocal Space Based Method for Treating Long Range Interactions in Ab Initio and Force-Field-Based Calculations in Clusters. *J. Chem. Phys.* **1999**, *110*, 2810–2821.
- (47) Bussi, G.; Donadio, D.; Parrinello, M. Canonical Sampling Through Velocity Rescaling. *J. Chem. Phys.* **2007**, *126*, 014101.
- (48) Vandevondele, J.; Krack, M.; Mohamed, F.; Parrinello, M.; Chassaing, T.; Hutter, J. Fast and Accurate Density Functional Calculations Using a Mixed Gaussian and Plane Waves Approach. *Comput. Phys. Commun.* **2005**, *167*, 103–128.
- (49) Wang, J.; Wolf, R. M.; Caldwell, J. W.; Kollman, P. A.; Case, D. A. Development and Testing of a General Amber Force Field. *J. Comput. Chem.* **2004**, *25*, 1157–1174.
- (50) Bayly, C. I.; Cieplak, P.; Cornell, W.; Kollman, P. A. A Well-Behaved Electrostatic Potential Based Method Using Charge Restraints for Deriving Atomic Charges: the RESP Mode. *J. Phys. Chem.* **1993**, *97*, 10269–10280.
- (51) Cornell, W. D.; Cieplak, P.; Bayly, C. I.; Kollmann, P. A. Application of RESP Charges to Calculate Conformational Energies,

Hydrogen Bond Energies, and Free Energies of Solvation. *J. Am. Chem. Soc.* **1993**, *115*, 9620–9631.

(52) Jorgensen, W. L.; Chandrasekhar, J.; Madura, J. D.; Impey, R. W.; Klein, M. L. Comparison of Simple Potential Functions for Simulating Liquid Water. *J. Chem. Phys.* **1983**, *79*, 926–935.

(53) Martyna, G. J.; Tobias, D. J.; Klein, M. L. Constant Pressure Molecular Dynamics Algorithms. *J. Chem. Phys.* **1994**, *101*, 4177–4189.

(54) Feller, S. E.; Zhang, Y.; Pastor, R. W.; Brooks, B. R. Constant Pressure Molecular Dynamics Simulation: The Langevin Piston Method. *J. Chem. Phys.* **1995**, *103*, 4613–4621.

(55) Nelson, M. T.; Humphrey, W.; Gursoy, A.; Dalke, A.; Kale, L. V.; Skeel, R. D.; Schulten, K. NAMD: A Parallel, Object Oriented Molecular Dynamics program. *Int. J. Supercomput. Appl. High Perform. Comput.* **1996**, *10*, 251–268.

(56) Ryckaert, J. P.; Ciccotti, G.; Berendsen, H. J. C. Numerical-Integration of Cartesian Equations of Motion of a System with Constraints – Molecular-Dynamics of n-Alkanes. *J. Comput. Phys.* **1977**, *23*, 327–341.

(57) Verlet, L. Computer “Experiments” on Classical Fluids. I. Thermodynamical Properties of Lennard-Jones Molecules. *Phys. Rev.* **1967**, *159*, 98–103.

(58) Verlet, L. Computer “Experiments” on Classical Fluids. II. Equilibrium Correlation Functions. *Phys. Rev.* **1968**, *165*, 201–214.

(59) Humphrey, W.; Dalke, A.; Schulten, K. VMD: Visual Molecular Dynamics. *J. Mol. Graphics Model.* **1996**, *14*, 33–38.

(60) Baker, N. A.; Sept, D.; Joseph, S.; Holst, M. J.; McCammon, J. A. Electrostatics of Nanosystems: Application to Microtubules and the Ribosome. *Proc. Natl. Acad. Sci. U.S.A.* **2001**, *98*, 10037–10041.

(61) Wagoner, J. A.; Baker, N. A. Assessing Implicit Models for Nonpolar Mean Solvation Forces: The Importance of Dispersion and Volume Terms. *Proc. Natl. Acad. Sci. U.S.A.* **2006**, *103*, 8331–8336.

(62) Kollman, P. A.; Massova, I.; Reyes, C.; Kuhn, B.; Huo, S.; Chong, L.; Lee, M.; Lee, T.; Duan, Y.; Wang, W.; et al. Calculating Structures and Free Energies of Complex Molecules: Combining Molecular Mechanics and Continuum Models. *Acc. Chem. Res.* **2000**, *33*, 889–897.

(63) Miller, B. R.; McGee, T. D.; Swails, J. M.; Homeyer, N.; Gohlke, H.; Roitberg, A. E. MMPBSA.py: An Efficient Program for End-State Free Energy Calculations. *J. Chem. Theory Comput.* **2012**, *8*, 3314–3321.

(64) McQuarrie, D. A. *Statistical Mechanics*, 2nd ed.; University Science Books: 2000.

(65) Grimme, S. Accurate Description of van der Waals Complexes by Density Functional Theory Including Empirical Corrections. *J. Comput. Chem.* **2004**, *25*, 1463–1473.

(66) Gonzalez, C.; Lim, E. C. Evaluation of the Hartree-Fock Dispersion (HFD) Model as a Practical Tool for Probing Intermolecular Potentials of Small Aromatic Clusters: Comparison of the HFD and MP2 Intermolecular Potentials. *J. Phys. Chem. A* **2003**, *107*, 10105–10110.

(67) Maritan, A.; Micheletti, C.; Trovato, A.; Banavar, J. R. Optimal Shapes of Compact Strings. *Nature* **2000**, *406*, 287–290.

(68) Chaires, J. B. Drug-DNA Interactions. *Curr. Opin. Struct. Biol.* **1998**, *8*, 314–320.

(69) Chaires, J. B. A Thermodynamic Signature for Drug-DNA Binding Mode. *Arch. Biochem. Biophys.* **2006**, *453*, 26–31.

(70) Spiegel, K.; Rothlisberger, U.; Carloni, P. Duocarmycins Binding to DNA Investigated by Molecular Simulations. *J. Phys. Chem. B* **2006**, *110*, 3647–3660.

(71) Vargiu, A. V.; Ruggerone, P.; Magistrato, A.; Carloni, P. Dissociation of Minor Groove Binders from DNA: Insights from Metadynamics Simulations. *Nucleic Acids Res.* **2008**, *36*, 5910–5921.